

Filling the holes: Evolving excised binary black hole initial data with puncture techniques

Zachariah B. Etienne,¹ Joshua A. Faber,^{1,*} Yuk Tung Liu,¹ Stuart L. Shapiro,^{1,†} and Thomas W. Baumgarte^{2,‡}

¹*Department of Physics, University of Illinois at Urbana-Champaign, Urbana, IL 61801*

²*Department of Physics and Astronomy, Bowdoin College, Brunswick, ME 04011*

(Dated: November 6, 2018)

We follow the inspiral and merger of equal-mass black holes (BHs) by the moving puncture technique and demonstrate that both the exterior solution and the asymptotic gravitational waveforms are unchanged when the initial interior solution is replaced by constraint-violating “junk” initial data. We apply this result to evolve conformal thin-sandwich (CTS) binary BH initial data by filling their excised interiors with arbitrary, but smooth, initial data and evolving with standard puncture gauge choices. The waveforms generated for both puncture and filled-CTS initial data are remarkably similar, and there are only minor differences between irrotational and corotational CTS BH binaries. Even the interior solutions appear to evolve to the same constraint-satisfying solution at late times, independent of the initial data.

I. INTRODUCTION

Numerical relativity has made dramatic progress over the past two years in solving the binary black hole (BBH) problem via the “moving puncture” technique [1, 2, 3]. To construct puncture initial data, the spatial metric is taken to be conformally flat and the conformal factor is split into an algebraic singular piece and a numerically determined regular contribution [4, 5]. These initial data are then evolved via the BSSN [6, 7] formulation of Einstein’s equations, *without* special treatment of the initial (coordinate) singularities at the punctures. Coupled to the BSSN field evolution equations are a set of gauge evolution equations, similar to those discussed in [8, 9] and successfully evolved by [1, 2], that are critical for long-term stability.

One possible reservation is that puncture initial data are thought to contain more inherent eccentricity [10] and, possibly, more initial spurious gravitational radiation than those constructed using the conformal thin-sandwich (CTS) method. CTS initial data are typically constructed with equilibrium boundary conditions imposed on an excised surface defining the BH horizon [11, 12, 13], and it has been suggested that the lack of data in the BH interior may pose a significant problem for evolving CTS initial data with puncture techniques (see, e.g., [14]). Thus, excision-based initial data, for both orbiting binaries [15, 16] and head-on collisions [17, 18], have heretofore been evolved via dynamical excision, rather than puncture techniques. We will demonstrate here that there are no difficulties evolving BH interiors artificially filled with smoothly extrapolated “junk”

(i.e., constraint-violating) initial data via puncture techniques: the puncture gauge conditions quickly drive the evolution toward the usual late-time puncture interior solutions, independent of the initial interior data.

This demonstration follows from several previous studies of BHs in puncture gauges. In [19, 20, 21], it was shown that the conformal factor ψ evolves from a $1/r$ dependence at small r to $1/\sqrt{r}$ at late times, indicating that the spatial slices terminate on a limiting surface of finite areal radius. It was argued in [22] that this effect is really a consequence of “excision via under-resolution”, namely the fact that the puncture gauge conditions make numerical grid points move away from the puncture very rapidly. In a Kruskal diagram, where the puncture is represented by the asymptotic end of region III, all grid points quickly move from region III into region II, leaving few or no grid points behind in the “left” part of the diagram (see Fig. 2 in [22]).

In a recent paper [23], we demonstrated that one can replace the solution inside the horizon of a single *stationary* puncture BH by “junk data”. We find that this junk does not affect the BH exterior and, more surprisingly, even in the black hole interior the BH settles down to the same constraint-satisfying solution, independently of the initial data. This can again be motivated with the help of a Kruskal diagram. We impose junk on the $t = 0$ slice in the black hole interior, i.e. in the “left” part of the diagram. As demonstrated by [22], the puncture gauge conditions make all grid points propagate toward the right at extremely rapid, “superluminal” speeds. Assuming that constraint violations travel with much smaller speeds, the grid points are likely to leave the junk’s future domain of dependence eventually, and enter a region that is affected by constraint-satisfying initial data only.

Here, we extend our work to the BBH case. We first demonstrate numerically that replacing interior puncture initial data by “junk” data does not alter the exterior evolution. Given this finding, we then show that the excised CTS initial data generated by Cook and Pfeiffer ([11]; hereafter CP) can be evolved using puncture gauges

*National Science Foundation (NSF) Astronomy and Astrophysics Postdoctoral Fellow.

†Also at Department of Astronomy and NCSA, University of Illinois at Urbana-Champaign, Urbana, IL 61801

‡Also at Department of Physics, University of Illinois at Urbana-Champaign, Urbana, IL 61801

without loss of accuracy by filling in the interior with arbitrary, but smooth, initial data. Rather than producing highly accurate waveforms, the goal of this paper is to establish a point of principle about initial data for dynamical evolutions.

II. INITIAL DATA

Throughout this paper we cast the spacetime metric g_{ab} into its 3+1 ADM form

$$ds^2 = -(\alpha^2 - \beta_i \beta^i) dt^2 + 2\beta_i dt dx^i + \psi^4 \tilde{\gamma}_{ij} dx^i dx^j, \quad (1)$$

with lapse function α , shift vector β^i , and spatial metric $\gamma_{ij} = \psi^4 \tilde{\gamma}_{ij}$, where $\tilde{\gamma}_{ij}$ is the conformally related metric and the conformal factor ψ is chosen so that $\det(\tilde{\gamma}) = 1$ in Cartesian coordinates. Both puncture and CP spatial initial data are conformally flat at $t = 0$, i.e., $\tilde{\gamma}_{ij} = \eta_{ij}$.

In generating BBH puncture initial data [4, 5], the momentum constraint reduces to an algebraic expression and the Hamiltonian constraint to a nonlinear elliptic equation governing the nonsingular part of ψ , which we solve via the **Lorene** multidomain spectral methods libraries [24]. These constraint equations depend on the initial linear momenta, coordinate separation, spins, and puncture masses. We obtain these initial parameters from the quasiequilibrium, circular sequence of [25], first treating the case of nonspinning, equal-mass BHs.

To better understand the role played by the BH interiors in puncture evolutions, we replace the puncture interiors (“P”) with “junk” initial data. Specifically, we replace the singular term of ψ with some other smooth function inside a radius r_J and leave the nonsingular part untouched, as we did in [23] for stationary BHs.

The singular part of ψ is $\psi_s = \sum_i (M_i/2r_i)$, where M_i is the puncture mass of BH i , and r_i is the distance from the origin to BH i . We construct *smooth junk* (“PSJ”) by replacing the term $M_i/2r_i$ by an even, fourth-order polynomial inside $r_J/M_i = 0.4$ (in these isotropic coordinates, the apparent horizon radius is located at $r_{\text{AH}} \approx 0.5M_i$ initially), chosen such that the resulting conformal factor is continuous and twice differentiable everywhere. *Flat junk* (“PFJ”) is defined by replacing $M_i/2r_i$ with a constant value 2.0 within $r_J/M_i = 0.25$. This second choice produces a conformal factor that is continuous, but not differentiable everywhere. Clearly, the the Hamiltonian constraint is *not* satisfied within the junk regions of our grid initially.

The corotating CP initial data (“CP_C”) are available from [26], whereas the irrotational CP data (“CP_I”) were graciously supplied by Harald Pfeiffer. Unlike puncture initial data, which are defined everywhere in space, CP initial data are produced by imposing equilibrium boundary conditions on excision surfaces – chosen to be coordinate spheres – that define the BH’s apparent horizons. This procedure produces valid data only in the BH exterior. To aide in some numerical simulations, the CP initial data were provided with data extrapolated from

TABLE I: Summary of parameters for our simulations. For initial data, “CP” refers to CTS Cook-Pfeiffer data, smoothly extrapolated inside the excised regions. M is the total ADM mass of the binary system, r_0 and J_0 the initial separation and total angular momentum, and M_{irr} the irreducible mass of each BH. ΔE and ΔJ are the total radiated energy and angular momentum during the course of the evolution in the dominant $l = 2$, $m = \pm 2$ modes, evaluated at extraction radii of $17.8M$.

Name	Init. Data	$M\Omega$	r_0/M	J_0/M^2	M_{irr}/M	$\Delta E/M$	$\Delta J/J_0$
P	No Junk	0.0824	2.185	0.807	0.476	0.026	0.16
PSJ	Sm. Junk	0.0824	2.185	0.807	0.476	0.027	0.17
PFJ	Flat Junk	0.0824	2.185	0.807	0.476	0.026	0.16
CP _I	Irrot. CP	0.0824	2.237	0.823	0.447	0.029	0.19
CP _C	Corot. CP	0.0817	2.222	0.877	0.444	0.028	0.19

the BH exterior to a region outside $0.75r_{\text{AH}}$. To fill the remaining excised region inside $0.75r_{\text{AH}}$, we extrapolate all field values radially from $0.8r_{\text{AH}}$ to the BH center, matching smoothly to fourth-order polynomials with a fixed, finite value at $r = 0$, so that the resulting field variables are everywhere continuous and twice differentiable, similar to the PSJ puncture case. Evolving with the CTS gauge variables α and β^i results in eccentric BH coordinate trajectories. We can remove this gauge-dependent eccentricity considerably by choosing instead the same initial lapse and shift as in the puncture cases, $\alpha = \psi^{-2}$ and $\beta^i = 0$, evolving with Eqs. (2) – (3) below.

In Table I, we summarize the parameters for each of our numerical simulations. Both irrotational and corotating CP data are evolved from an initial separation $r_0 \approx 2.2M$, which is beyond the quasiequilibrium ISCO radius, and comparable to the initial configurations evolved in [1, 2]. Here and below M is the binary’s total ADM mass. For comparison, we construct puncture initial data with the same orbital frequency as the irrotational CP data ($M\Omega = 0.08241$), using the equal-mass irrotational fitting formulae of [25] to determine our initial parameters. All runs were performed on $420^2 \times 210$ spatial grids, assuming equatorial symmetry. We employ multiple-transition fisheye coordinates [1] to expand the physical extent of our grid, as we did in [23]. Our grid includes three 1:4 fisheye transitions at $r/M = 3.89, 5.22$, and 6.55 , all with transition width $s/M = 0.417$. Resolution in the innermost region is set to $M/24$, so the outer boundary falls at a physical distance of $\approx 170M$.

III. DYNAMICAL CALCULATIONS

Our evolutions are performed using the same Cactus-based [27] GRMHD code described in [23], but with the MHD matter and E&M field sectors disabled. Our originally second-order Iterative Crank-Nicholson BSSN-based code has been upgraded to fourth-order accurate spatial differencing with upwind differencing for advective

tive terms, but we still use second-order differencing for the time evolution.

We use standard puncture gauge evolution equations, specifically a 1 + log lapse and a “non-shifting shift”:

$$\partial_t \alpha = \beta^j \partial_j \alpha - 2\alpha K \quad (2)$$

$$\partial_t \beta^i = (3/4)B^i; \quad \partial_t B^i = \partial_t \tilde{\Gamma}^i - \eta B^i \quad (3)$$

where we set $\eta = 0.5/M$ in all of our runs.

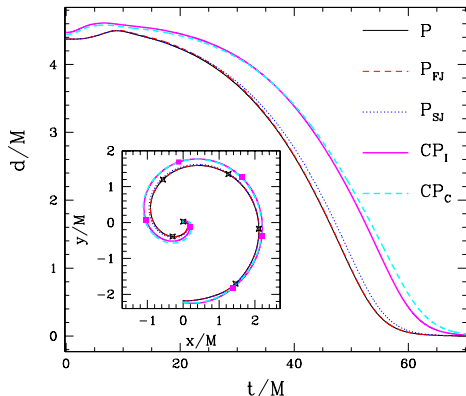


FIG. 1: Binary separation versus time and paths traced in coordinate space (inset) for runs P (thin solid), P_{FJ} (thin dashed), P_{SJ} (thin dotted), CP_I (thick solid), and CP_C (thick dashed). In the inset, we show the motion of one of the BHs in the equatorial plane, with points representing positions every $10M$ for runs P (open squares) and CP_I (closed squares). While π -symmetry is not enforced, it holds true numerically during our evolutions.

In Fig. 1, we show the coordinate trajectories of one of the punctures, which obey the relation $dx^i/dt = -\beta^i(x^i)[1]$. For runs with non-singular junk data in the interior, we locate the initial BH position at $r = 0$, coincident with the standard puncture case. While the puncture and CP runs trace out slightly different tracks, this comparison is gauge-dependent. To evaluate our runs in an asymptotically gauge-invariant manner, we compute the gravitational waveforms through the Weyl scalar ψ_4 via the Cactus PsiKadellia thorn [28], which we have modified to make the computation of spatial derivatives accurate to fourth order. We have tested our modified PsiKadellia thorn with a full suite of analytic linearized wave tests. The total energy and angular momentum lost to gravitational radiation are computed by integrating Eqs. (5.1) and (5.2) in [29], keeping only the $s = -2$ spin-weighted, $l = 2$, $m = \pm 2$ contributions from ψ_4 to reduce numerical noise. We have performed simulations at various resolutions using the same puncture initial data as in [1], finding that our waveform agrees with Fig. 3 of the preprint version of [1] to high accuracy, and converges to second order, as we show in Fig. 3 for the CP_I case.

In [23], we demonstrated that even if single stationary punctures are constructed with different junk initial interior data, the ADM mass versus time and conformal

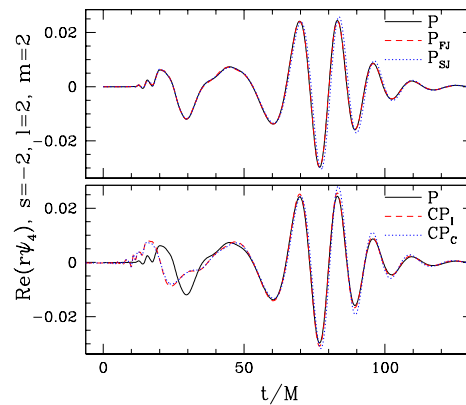


FIG. 2: Real part of the $s = -2$ spin-weighted, $l = 2$, $m = 2$ component of the Weyl scalar ψ_4 , evaluated on a sphere of radius $r = 17.8M$. In the top panel we show results for puncture runs P (solid), P_{FJ} (dashed), and P_{SJ} (dotted), which differ in the form of the initial junk we impose within each BH horizon. In the bottom panel, we compare run P with our two runs started from CP initial data, both irrotational (dashed) and corotating (dotted). We see extremely close agreement between puncture and irrotational CP results, and only minor differences between these and the corotating CP results.

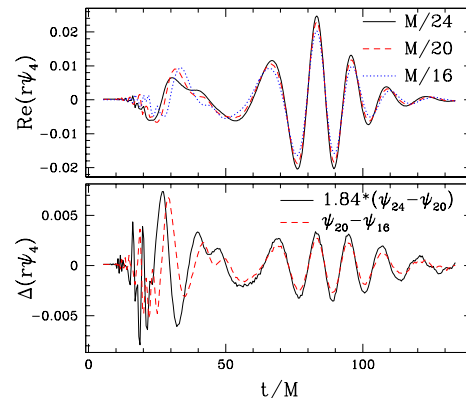


FIG. 3: Waveforms for runs using the initial data of run CP_I (top panel) evaluated at numerical resolutions of $M/24$ (solid), $M/20$ (dashed), and $M/16$ (dotted). Results are time and phase shifted so that the moment and phase of the maximum wave amplitudes coincide. In the bottom panel, we show the differences between the runs, properly rescaled to highlight second-order convergence.

factor profiles at late times agree to high accuracy. Here, we demonstrate that the gravitational waveforms generated by puncture BBHs are also largely independent of interior junk. In Fig. 2, we show the real $l = 2$, $m = 2$ -mode component of ψ_4 , evaluated on a sphere of physical (as opposed to fisheye) radius $r = 17.8M$, comparable to the extraction radius used in [1, 2]. In the top panel, we show a comparison between simulations P, P_{FJ} , and P_{SJ} . We find that the first two cases are almost identical, even though the data P_{FJ} are not differentiable initially in the

BH interior. There is a slight phase difference for run P_{SJ} , since the differencing stencil in the inner edge of the exterior overlaps junk data in the interior that do not initially satisfy the constraints. In the bottom panel of the figure, we compare results from simulation P with those from CP initial data (the CP curves are time and phase-shifted equally so that the time and phase at maximum amplitude match between runs P and CP_I). We note that after an early phase of transient gravitational radiation propagation, the waveforms from the merger and ring-down of runs P and CP_I match very closely, varying in amplitude by no more than 4% with nearly exact phase agreement. These relative differences are well within the relative differences in the initial data's masses and angular momenta, as listed in Table I.

The similarity between puncture and CP merger waveforms may not be particularly surprising, since the gauge evolution equations inevitably drive a BH toward the universal form described in [19]. To demonstrate this effect, in Fig. 4 we compare profiles of $r\psi^2$ for runs P and CP_I at $t = 0$ and $20M$, before coalescence. In both cases, the gauge conditions we choose drive the solution toward $\psi \propto r^{-1/2}$, regardless of whether the initial data are singular or expressly finite. For an isolated BH, it was shown in [19] that the puncture $r = 0$ evolves to a limiting slice of finite Schwarzschild radius, $r_s = \psi^2 r \approx 1.3M$. We observe the same asymptotic value for this function in all of our binary evolutions prior to coalescence.

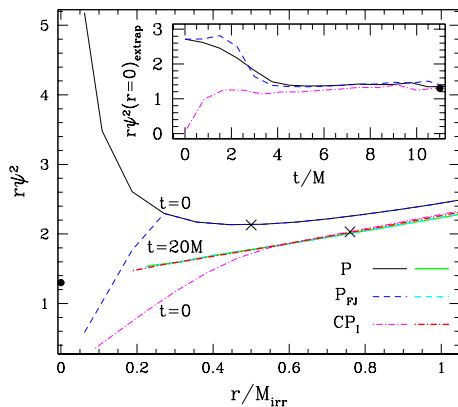


FIG. 4: Radial profiles of the quantity $r\psi^2$ as a function of coordinate radius, measured out from the BH center for runs P and CP_I . The evolution inevitably drives ψ toward the power-law index $\psi \propto r^{-1/2}$ derived in [19]. For the curves showing profiles at $t = 20M$, we eliminate the two innermost points, whose values are inaccurate due to differencing across the puncture. Crosses denote the initial apparent horizons for each run. In the inset, we plot the value of $r\psi^2$ linearly extrapolated from the third and fourth innermost data points as a function of time for the same runs. The filled circles show the asymptotic value $1.3M$ determined analytically by [19].

In Fig. 5, we compare the magnitude of the normalized constraint violations [30] for different initial data sets, summing over spherical shells about each puncture spanning $0.2 < r/M < 0.3$. These shells allow us to study

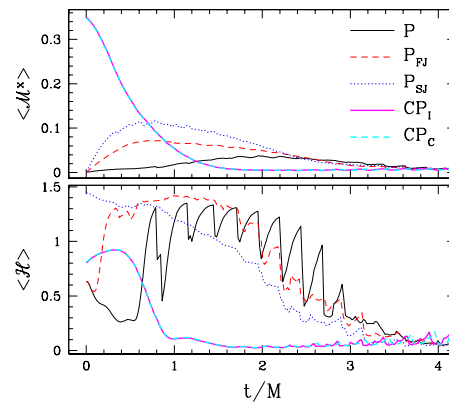


FIG. 5: Violation of the Hamiltonian ($\mathcal{H} = 0$) and momentum ($\mathcal{M}^i = 0$) constraints. We show the normalized x-component of the momentum constraint violation $\langle \mathcal{M}^x \rangle \equiv \sqrt{\sum (\mathcal{M}^x)^2} / N_{MC}$ (top panel), where N_{MC} is the L_2 -norm of \mathcal{M}^x given by Eq. 60 of [30], and a similar quantity for the Hamiltonian constraint (bottom panel). These are summed over spherical shells about each puncture $0.2 < r/M < 0.3$, which extend into the BH interiors. The constraint-violating initial data are driven to constraint-satisfying solutions at late times (several M).

constraint violations propagating outward in the immediate vicinity of the BHs, the exterior region most sensitive to the use of interior junk. We find a brief but transient increase in the magnitude of the violations at early times in all the puncture simulations, whereas the CP simulations begin with larger violations but are driven toward constraint-satisfying configurations quite rapidly.

IV. DISCUSSION

For solutions of Einstein's equations, the BH exterior must, by definition, be independent of the BH interior. As long as constraint violations propagate “causally”, this must also be true if the BH interior violates the constraints (see the subsequent discussion in [31]). Previous analyses [19, 20, 21, 22] also suggest that, with the “moving puncture” gauges, any initial BH configuration would be driven to the asymptotic puncture solution found in [19]. We demonstrate numerically that this is indeed the case and show that one can modify the data within the BH interior and produce valid waveforms. The success of the puncture method does not depend on the form of the initial data, or even on the existence of valid initial data, in the BH interior.

More specifically, we find that evolutions of puncture initial data are insensitive to interior “junk” so long as the finite differencing stencils of exterior points do not overlap regions where constraints are violated. One may freely modify the interior fields to eliminate initially asymptotic singular behavior, or even invent initial data in the interior if they do not exist, so long as the solution

matches smoothly to the exterior so that all fields are twice differentiable and satisfy the constraints in regions covered by the differencing stencils of exterior points.

As a consequence, excised initial data, in particular the CTS sets constructed in [11, 12, 13], may be evolved using puncture techniques. These data produce a different initial burst of spurious gravitational radiation, reflecting small differences in the “imperfection” of the initial data, but evolve similarly to punctures thereafter. This is true for both irrotational and corotating CTS data. The differences are small since the latter involve only marginally spinning BHs ($S/M_{\text{irr}}^2 = 0.15$). In fact, all our waveforms are very similar, and any relative differences in the wave signals are well within the relative differences of the physical parameters describing the initial data.

These results are also highly relevant for black hole-neutron star (BHNS) binary evolutions. To date, most published relativistic quasiequilibrium BHNS sequences are calculated using the CTS method and excision [32, 33, 34] (the exception are the puncture data constructed in [35, 36]). As demonstrated in this paper, these data

can nevertheless be evolved with the moving puncture technique by appropriately filling the excised region.

Finally, we note that the interior metric seems to evolve to the same asymptotic form found by [19], independently of the initial interior data. Consequently, the late-time interior solutions on the numerical grid satisfy the constraints with increasing accuracy, even if the initial data consist of constraint-violating “junk” (see Fig. 5). This feature presumably helps stabilize the integrations and explains the robustness of the puncture approach.

We are very grateful to H. Pfeiffer for providing us with irrotational CTS Cook-Pfeiffer initial data. We also thank G. Cook and Y. Zlochower for helpful conversations. JAF is supported by an NSF Astronomy and Astrophysics Postdoctoral Fellowship under award AST-0401533. This work was supported in part by NSF grants PHY-0205155 and PHY-0345151 and NASA Grants NNG04GK54G and NNX07AG96G to the University of Illinois, and NSF Grant PHY-0456917 to Bowdoin College. All simulations were performed on the NCSA *abe* cluster.

-
- [1] M. Campanelli, C. O. Lousto, P. Marronetti, and Y. Zlochower, *Phys. Rev. Lett.* **96**, 111101 (2006).
- [2] J. G. Baker, J. Centrella, D.-I. Choi, M. Koppitz, and J. van Meter, *Phys. Rev. Lett.* **96**, 111102 (2006).
- [3] For an alternate method, see F. Pretorius, *Phys. Rev. Lett.* **95**, 121101 (2005).
- [4] S. Brandt and B. Brügmann, *Phys. Rev. Lett.* **78**, 3606 (1997).
- [5] T. W. Baumgarte, *Phys. Rev. D* **62**, 024018 (2000).
- [6] M. Shibata and T. Nakamura, *Phys. Rev. D* **52**, 5428 (1995).
- [7] T. W. Baumgarte and S. L. Shapiro, *Phys. Rev. D* **59**, 024007 (1999).
- [8] C. Bona, J. Massó, E. Seidel, and J. Stela, *Physical Review Letters* **75**, 600 (1995), arXiv:gr-qc/9412071.
- [9] M. Alcubierre, B. Brügmann, P. Diener, M. Koppitz, D. Pollney, E. Seidel, and R. Takahashi, *Phys. Rev. D* **67**, 084023 (2003), arXiv:gr-qc/0206072.
- [10] E. Berti, S. Iyer, and C. M. Will, *Phys. Rev. D* **74**, 061503 (2006).
- [11] G. B. Cook and H. P. Pfeiffer, *Phys. Rev. D* **70**, 104016 (2004).
- [12] M. Caudill, G. B. Cook, J. D. Grigsby, and H. P. Pfeiffer, *Phys. Rev. D* **74**, 064011 (2006).
- [13] H. P. Pfeiffer, D. A. Brown, L. E. Kidder, L. Lindblom, G. Lovelace, and M. A. Scheel, *Class. Quant. Grav.* **24**, 59 (2007).
- [14] S. Husa, J. A. Gonzalez, M. Hannam, B. Bruegmann, and U. Sperhake, ArXiv e-prints (2007), 0706.0740.
- [15] J. G. Baker, M. Campanelli, F. Pretorius, and Y. Zlochower, *Class. Quant. Grav.* **24**, 25 (2007).
- [16] J. Thornburg, P. Diener, D. Pollney, L. Rezzolla, E. Schnetter, E. Seidel, and R. Takahashi, ArXiv e-prints (2007), gr-qc/0701038.
- [17] U. Sperhake, ArXiv e-prints (2006), gr-qc/0606079.
- [18] U. Sperhake, B. Bruegmann, J. Gonzalez, M. Hannam, and S. Husa, ArXiv e-prints (2007), 0705.2035.
- [19] M. Hannam, S. Husa, D. Pollney, B. Brügmann, and N. O’Murchadha, ArXiv e-prints (2006), gr-qc/0606099.
- [20] M. Hannam, S. Husa, B. Brügmann, J. A. González, U. Sperhake, and N. Ó. Murchadha, *J. Phys. Conf. Series* **66**, 2047 (2007).
- [21] T. W. Baumgarte and S. G. Naculich, *Phys. Rev. D* **75**, 067502 (2007).
- [22] J. D. Brown, ArXiv e-prints (2007), 0705.1359.
- [23] J. A. Faber, T. W. Baumgarte, Z. B. Etienne, S. L. Shapiro, and K. Taniguchi, *Phys. Rev. D* (2007), submitted, 0708.2436.
- [24] <http://www.lorene.obspm.fr/>.
- [25] W. Tichy and B. Brügmann, *Phys. Rev. D* **69**, 024006 (2004).
- [26] <http://www.black-holes.org/researchers3.html>.
- [27] <http://www.cactuscode.org/>.
- [28] We define the normalization of the tetrad to agree with that used in [15].
- [29] J. Baker, M. Campanelli, C. O. Lousto, and R. Takahashi, *Phys. Rev. D* **65**, 124012 (2002).
- [30] M. D. Duez, P. Marronetti, S. L. Shapiro, and T. W. Baumgarte, *Phys. Rev. D* **67**, 024004 (2003).
- [31] D. Brown, O. Sarbach, E. Schnetter, M. Tiglio, P. Diener, I. Hawke, and D. Pollney, ArXiv e-prints (2007), 0707.3101.
- [32] K. Taniguchi, T. W. Baumgarte, J. A. Faber, and S. L. Shapiro, *Phys. Rev. D* **74**, 041502(R) (2006).
- [33] K. Taniguchi, T. W. Baumgarte, J. A. Faber, and S. L. Shapiro, *Phys. Rev. D* **75**, 084005 (2007).
- [34] P. Grandclément, *Phys. Rev. D* **74**, 124002 (2006).
- [35] M. Shibata and K. Uryu, *Class. Quant. Grav.* **24**, 125 (2007).
- [36] M. Shibata and K. Uryu, *Phys. Rev. D* **74**, 121503 (2006).